ISCI, Volume *12*

Supplemental Information

Structure of Human Mitochondrial Translation Initiation Factor 3 Bound to the Small Ribosomal Subunit

Ravi K. Koripella, Manjuli R. Sharma, Md. Emdadul Haque, Paul Risteff, Linda L. Spremulli, and Rajendra K. Agrawal

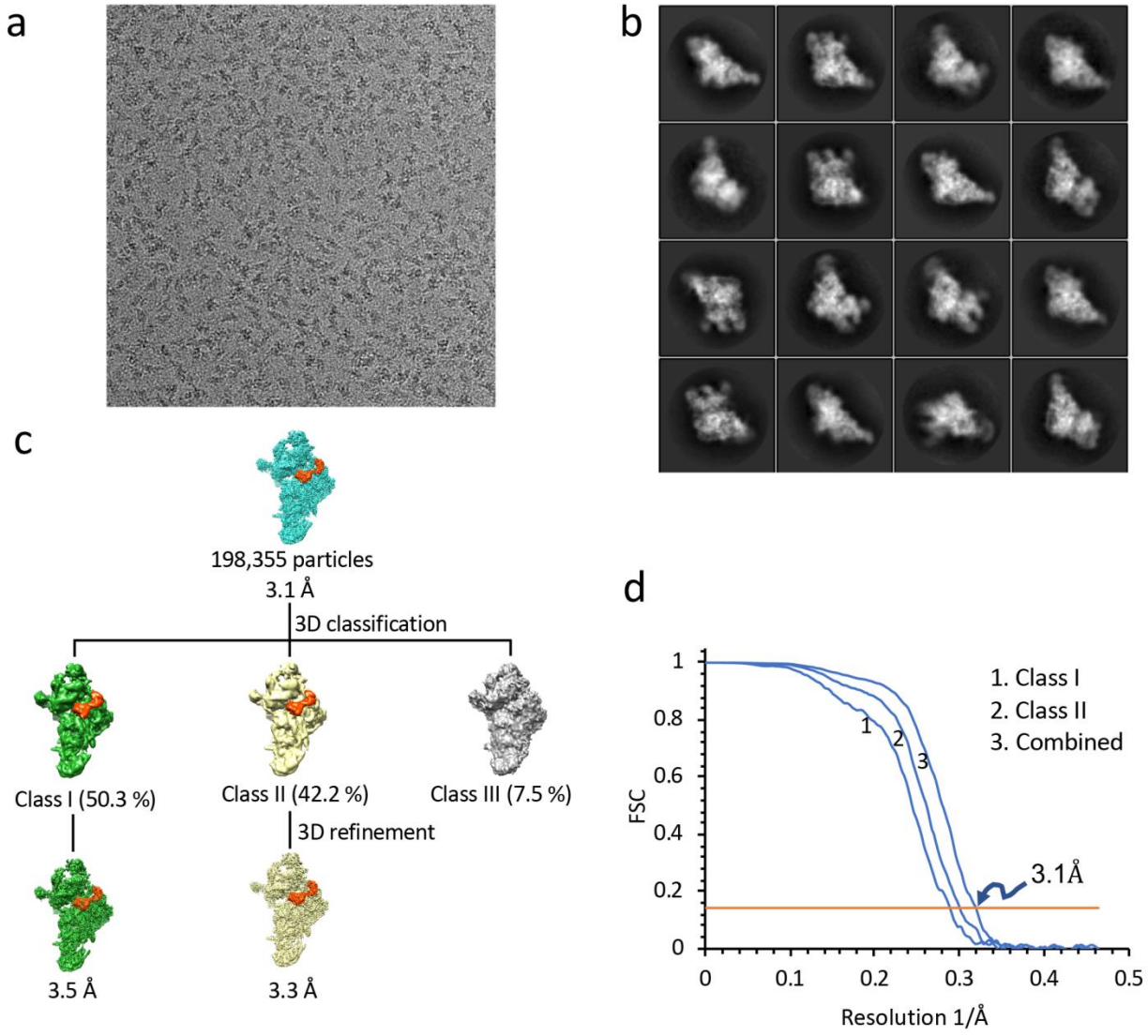

Figure. S1. Image processing of the 28S-IF3$_{mt}$ complex, Related to Figure 1 and Transparent Methods**.** (**a**) A typical electron micrograph showing the bovine mitochondrial 28S subunit in complex with human IF3$_{mt}$. (**b**) Representative two-dimensional (2D) class averages used in three-dimensional (3D) reconstructions. (**c**) Flow-chart showing results of 3D classification and refinements. A total of 198,355 particles corresponding to the selected 2D averages were refined to 3.1 Å. To remove conformational heterogeneity, the particles were subjected to 3D classification that yielded three different classes. After discarding the poorly aligned particles (Class III), particles corresponding to the other two classes were independently refined, to 3.5 Å (Class I), and 3.3 Å (Class II) (**d**) Fourier-shell correlation (FSC) curves of the final two maps that were used in our analysis.

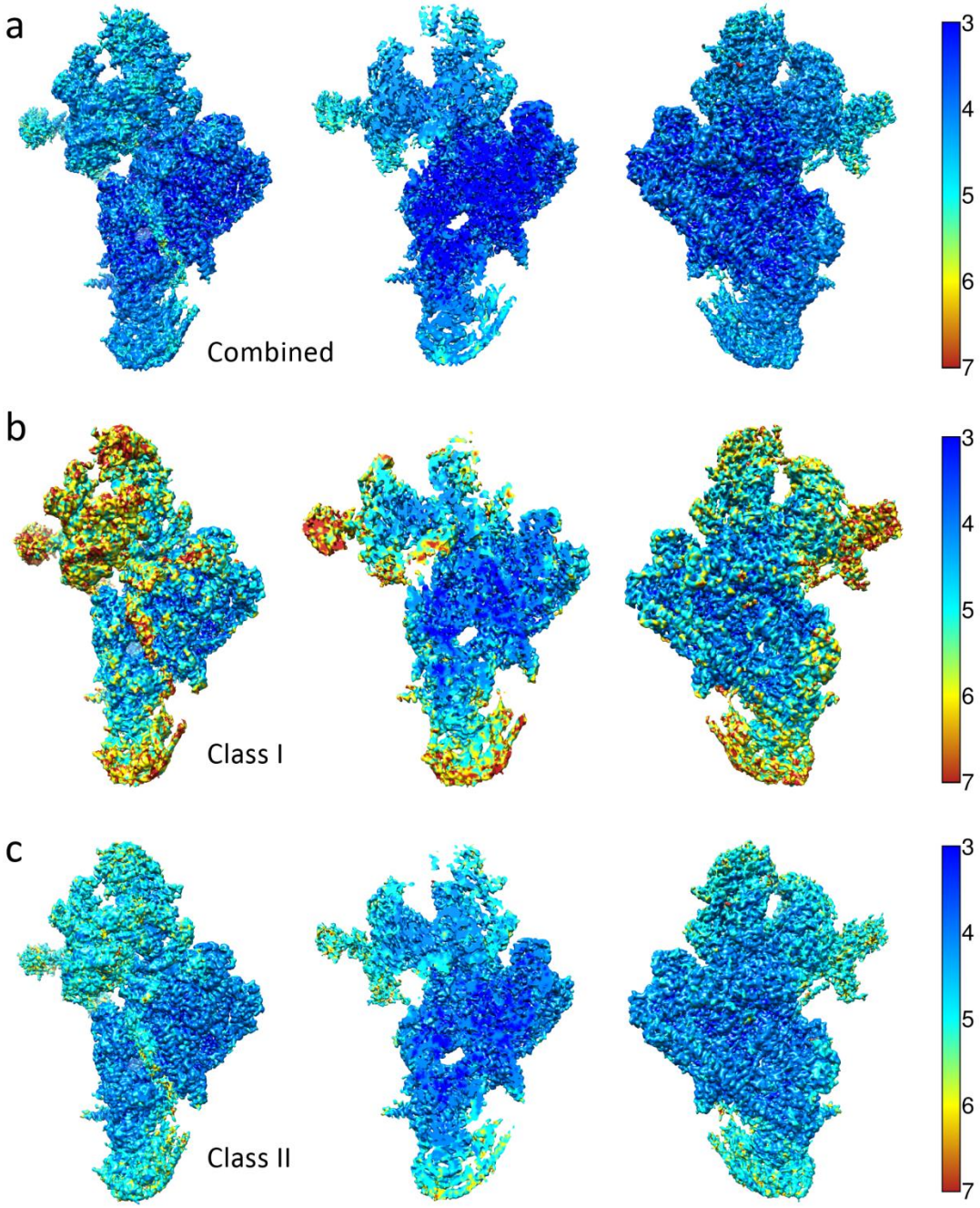

Figure. S2. Local resolution maps, Related to Figures 1, 2 and 3, and Transparent Methods**.** Local resolution for (**a**) the map obtained from full dataset, (**b**) Class I, and (**c**) Class II. Left panels show the local resolution maps as viewed from the subunit interface side, middle panels depict the core regions, after applying cutting planes, and right panels represent the view from the back side. Maps are color coded according to resolution bars shown on the extreme right.

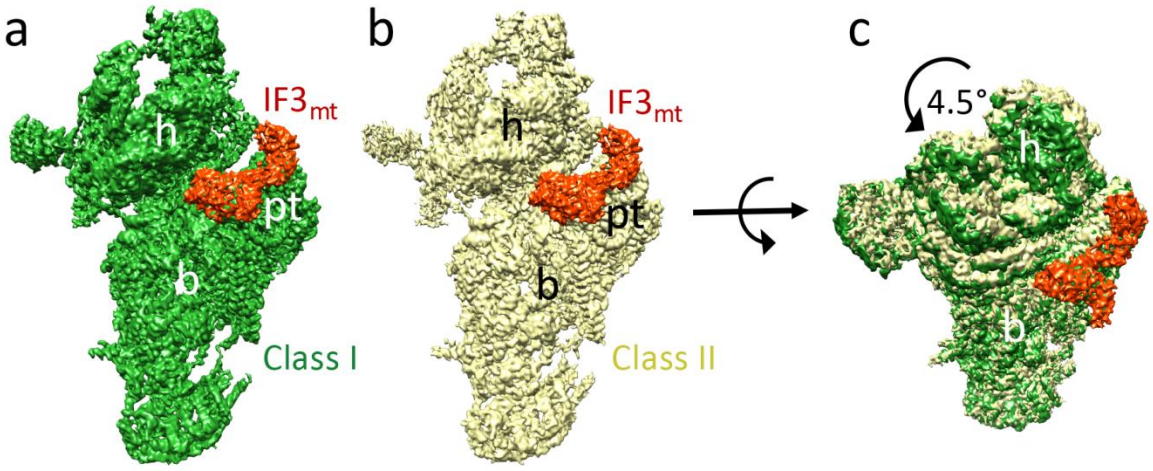

Figure. S3. Rotation of the 28S head relative to the platform region, Related to Figure 1**.** (**a**) Cryo-EM maps of class I (green) and (**b**) class II (yellow) with bound IF3$_{mt}$ (orange). Landmarks of the 28S subunit: h, head, b, body, and pt, platform. (**c**) Superimposition of class I with class II reveals an overall ~ 4.5 ° rotation of the 28S head in Class I, away from the platform region.

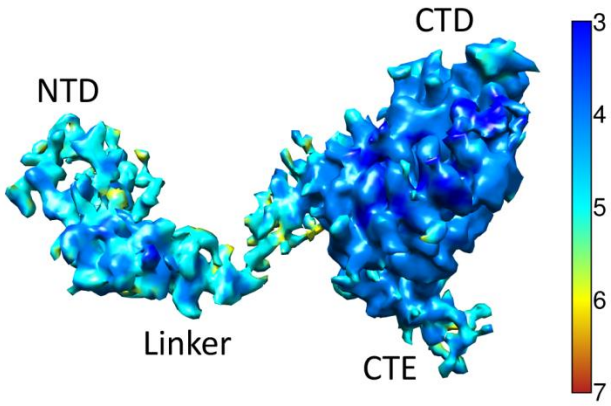

Figure. S4. Local resolution map of IF3$_{mt}$, Related to Figures 1 and 2**.** Local resolution for the density corresponding to IF3$_{mt}$ extracted from the cryo-EM map of the 28S-IF3$_{mt}$ Class II complex.

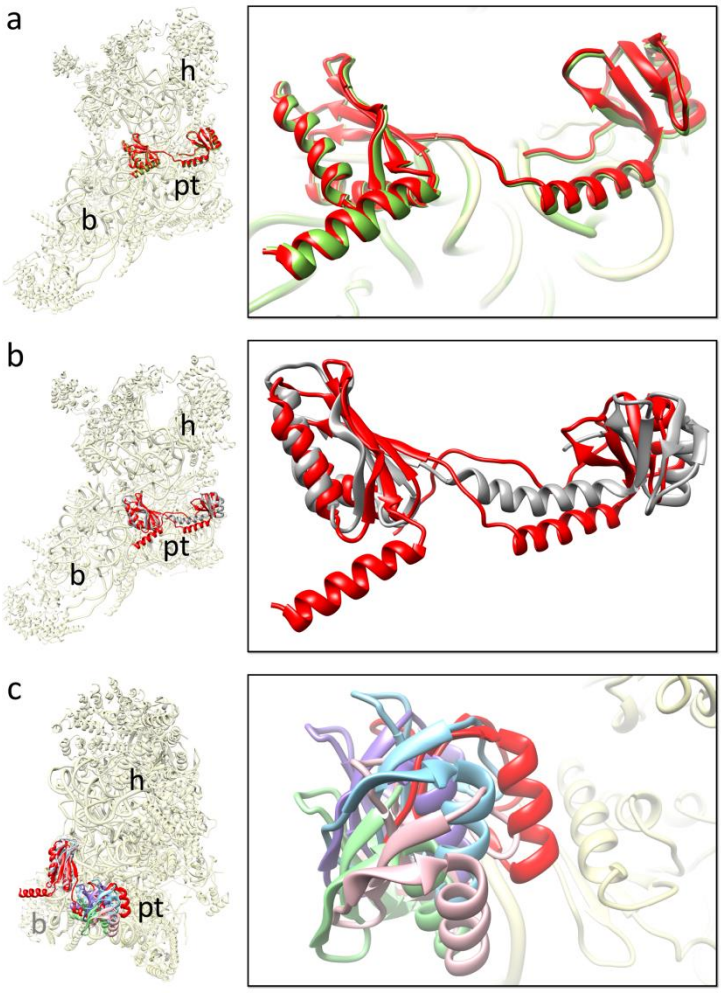

Figure. S5. Position of IF3$_{mt}$ NTD and CTD on the 28S subunit, Related to Figures 1 and 2**.** (**a**) The overall binding position of IF3$_{mt}$ in class I (green) and class II (red) remained almost identical, though the conformation of the 28S head domain is significantly different between these classes (Fig. S3). (**b**) Structures of the human IF3$_{mt}$ (red) and the bacterial IF3 (grey) (Hussain et al., 2016) superimposed. (**c**) The NTD of IF3$_{mt}$ (red) is positioned uniquely on the 28S subunit, as compared to the positions of NTD of the bacterial factor on the 30S subunit captured in four conformational states (lighter shades of green, purple, pink and blue) (Hussain et al., 2016; Lopez-Alonso et al., 2017). Thumbnails to the left represent overlaid positions of the ligands relative to the overall orientation to the 28S subunit (yellow). Landmarks on the thumbnail: h, head, b, body, and pt, platform.

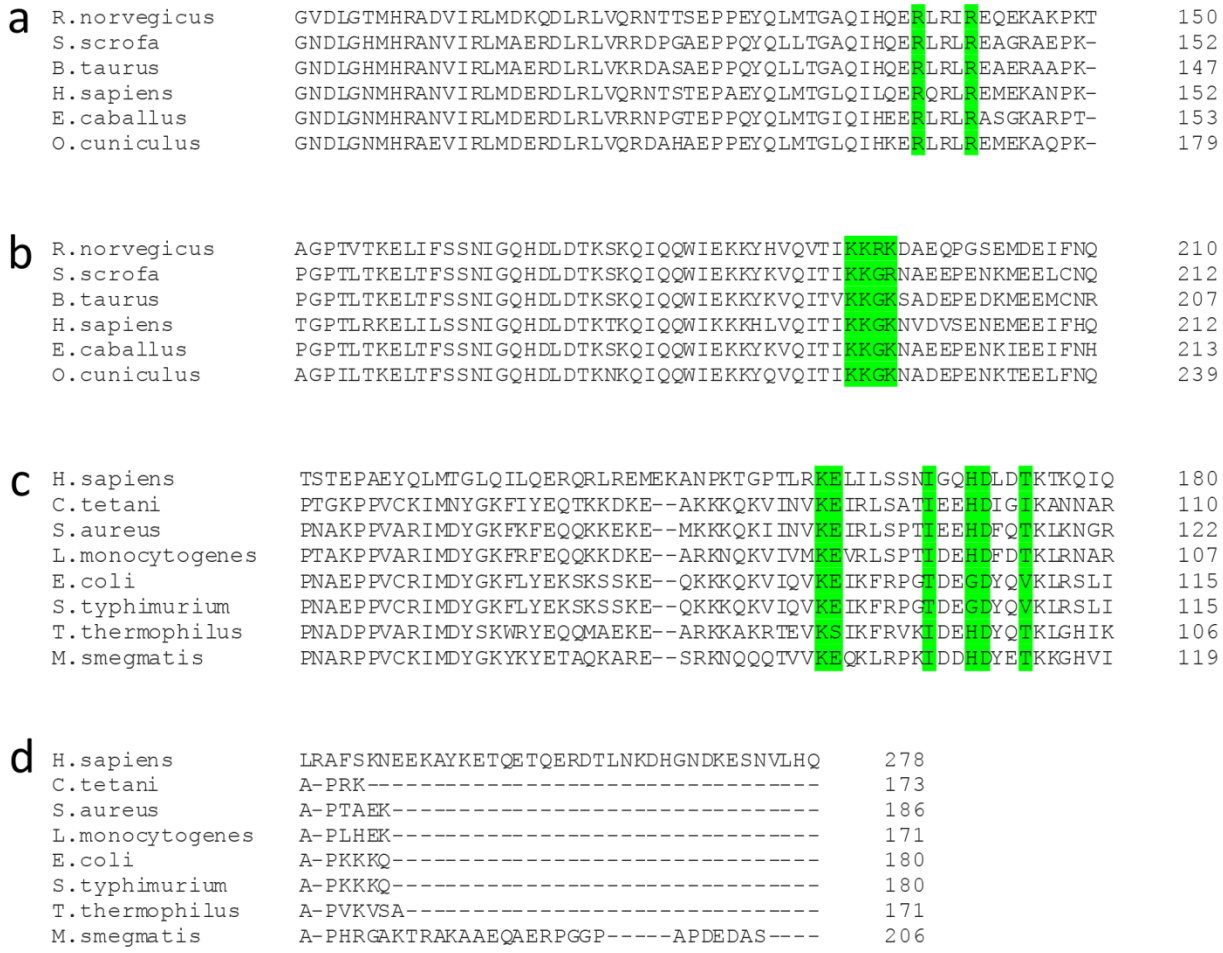

Figure. S6. Sequence alignment of mitochondrial IF3 homologues, Related to Figures 2, 3, and 6**.** Sequence alignment of select segments of (**a**, **b**) human $IF3_{mt}$ with other mammalian homologues, and (**c, d**) with bacterial homologues.

Figure. S7. Alignment of interacting segments of the 28S subunit components and IF3$_{mt}$ in human and bovine, Related to Figure 5**.** Select segments of (**a**) the 12S rRNA (**b**) MRP uS11 and (**c**) IF3$_{mt}$.

Table S1. Data Collection, Refinement and Model Validation, Related to Figures 1, 2, and 3, and Transparent Methods.

Description	**28S-IF3$_{mt}$ (Class I)**	**28S-IF3$_{mt}$ (Class II)**
Data collection and Refinement		
Microscope	FEI Titan Krios	
Voltage (kV)	300	
Pixel size (Å)	1.07	1.07
Defocus range (μm)	-1 to -3	-1 to -3
Average e^- dose per image ($e^-/Å^2$)	70.0	70.0
Software	RELION /cryoSPARC	RELION /cryoSPARC
Particles (initial)	198,355	198,355
Particles (final)	99,178	83,508
Symmetry	C1	C1
FSC-threshold	0.143	0.143
Resolution (Å)	3.48	3.32
Map-sharpening *B* factor ($Å^2$) overall	87.0	97.9
RMS deviations		
Bonds lengths (Å)	0.001	0.001
Bonds angles (^{o})	0.5	0.37
Molprobity clashscore	1.73 (88th)	1.70 (89th)
Clashscore, all atoms	3.23 (97th)	2.92 (98th)
Rotamer outliers (%)	0.06	0.04
Ramachandran plot		
Favored (%)	87.34	87.21
Outliers (%)	1.46	1.81
RNA		
Correct sugar puckers (%)	99.79	99.26
Angle outliers (%)	0.00	0.00
Bond outliers (%)	0.00	0.00
Good backbone conformations (%)	75.53	77.1
Model composition		
RNA bases Protein residues	952 5,482	952 5,482

Transparent Methods

Preparation of the 28S-IF3$_{mt}$ Complex: The mature form of human IF3$_{mt}$ was expressed and purified as described previously (Koc and Spremulli, 2002). Bovine mitochondrial 28S ribosomal subunits were prepared as described previously (Spremulli, 2007). Complexes containing IF3$_{mt}$ bound to 28S subunits were assembled in reaction mixtures (20 µL) containing 1 µM 28S subunits, 10 µM IF3$_{mt}$, 50 mM Tris-HCl, pH 7.6, 40 mM KCl, 7.5 mM $MgCl_2$, 10% glycerol, 2 mM dithiothreitol and 0.1 mM spermine. Reaction mixtures were incubated for 20 min at 25 ^{o}C, divided into 5 µL aliquots, fast-frozen in a dry ice isopropanol bath and stored at -70 ^{o}C. The amount of IF3$_{mt}$ bound to the 28S subunits was measured using a quantitative immuno dot blot using antibodies to bovine IF3$_{mt}$ as described previously (Haque and Spremulli, 2008). This analysis indicated that the complexes contained greater than 0.9 mol IF3$_{mt}$/mol 28S subunits. For cryo-EM analysis, the 28S-IF3$_{mt}$ complex was diluted to 100 nM with buffer containing 10 mM Tris-HCl, pH 7.6, 20 mM $MgCl_2$, 40 mM KCl, 1 mM DTT, 0.1 mM spermine and 5% glycerol, and then incubated for five min at 37°C prior to loading on the grids.

Cryo-Electron Microscopy and Image Processing: Home-made carbon was coated as a continuous layer (~ 50 Å thick) onto Quantifoil holey copper 1.2/1.3 grids, which were then glow-discharged for 30 s on a plasma sterilizer. After loading 4 µl of the sample to the grids, they were incubated for 15 s at 4°C and 100% humidity and then blotted for 4 s before flash-freezing into the liquid ethane using a Vitrobot (FEI). Data was acquired on a Titan Krios electron microscope equipped with a Gatan K2 summit direct-electron detecting camera at 300 KV. A defocus range of -1.0 to -3.0 µm was used at a calibrated magnification of 22,500 X, yielding a pixel size of 1.07 pixels Å on the object scale. A dose rate of 7 electrons per pixel per s and an exposure time of 10 s resulted in a total dose of 70 e$Å^{-2}$. Out of the 2,435 micrographs that were collected, 2,095 were selected after determining their contrast transfer function (CTF) using CTFFIND3 (Rohou and Grigorieff, 2015). The data was then processed in Relion 2.0 (Scheres, 2012) where a total of 320,824 particles were picked using its autopick function. All the downstream steps including 2D classification, 3D

classification and 3D refinement were performed using CryoSPARC (Punjani et al., 2017). After reference-free 2D classification, 198,355 good particles were selected, and refined to a resolution of 3.1 Å. The map showed strong IF3$_{mt}$ density, but the 28S head region appeared to contain heterogeneity. Therefore, the dataset was subjected to an initial reference-based heterogenous 3D classification (Fig. S1). 3D classification yielded two major classes that turned out to be 28S-IF3$_{mt}$ complexes that showed conformational differences in their head regions and a minor class that contained mostly deformed ribosomal particles that could not be processed further. 3D refinement was performed on the two major classes that yielded a final resolution of 3.5 Å for Class I (99,178 particles) and 3.3 Å for Class II (83,508 particles) (Figs. S1 and S2).

Model Building: Coordinates from the published bovine 28S subunit (Kaushal et al., 2014; PDB ID: 3JD5) were docked independently as rigid bodies into the corresponding cryo-EM density maps of Class I and Class II using Chimera 1.11 (Pettersen et al., 2004). The models were subsequently refined and validated in PHENIX (Adams et al., 2010) using the real-space refinement function. Initial homology models for human IF3$_{mt}$ were obtained from the Robetta server (Kim et al., 2004). The homology models were then placed independently as rigid bodies into the region of density map corresponding to the IF3$_{mt}$ using Chimera 1.11 (Pettersen et al., 2004), and the model that showed optimal fitting were selected. Portions of the homology model that could not be explained by the cryo-EM density corresponding to IF3$_{mt}$ were modelled in Chimera, based on the recognizable secondary structural elements (SSEs) and bulky side-chains of the amino acids in the cryo-EM map. The mito-specific C-terminal extension (CTE) was built *de novo* in Chimera 1.11 (Pettersen et al., 2004), guided by SSEs and position of the side-chains, and Coot (Emsley et al., 2010). Low resolution in the region of the cryo-EM map corresponding to the mito-specific N-terminal extension (NTE) restricted us from modelling the complete NTE, but the carbon backbone. The final model was refined for optimal fitting into the density map and further validated in PHENIX (Adams et al., 2010). The statistics of EM reconstructions and molecular modeling is provided in Table S1.

Data Availability: Both cryo-EM maps of the 28S subunit of the mammalian (*Bos taurus*) mitochondrial ribosome bound to human IF3 have been deposited in the Electron Microscopy and PDB Data Bank (wwPDB.org) under accession codes EMD-9362 and PDB ID 6NF8 for Complex I and under accession codes EMD-9358 and PDB ID 6NEQ for Complex II.

Supplemental References:

Adams, P.D., Afonine, P.V., Bunkoczi, G., Chen, V.B., Davis, I.W., Echols, N., Headd, J.J., Hung, L.W., Kapral, G.J., Grosse-Kunstleve, R.W.*, et al.* (2010). PHENIX: a comprehensive Python-based system for macromolecular structure solution. Acta Crystallogr D Biol Crystallogr *66*, 213-221.

Emsley, P., Lohkamp, B., Scott, W.G., and Cowtan, K. (2010). Features and development of Coot. Acta Crystallogr D Biol Crystallogr *66*, 486-501.

Haque, M.E., and Spremulli, L.L. (2008). Roles of the N- and C-terminal domains of mammalian mitochondrial initiation factor 3 in protein biosynthesis. J Mol Biol *384*, 929-940.

Hussain, T., Llacer, J.L., Wimberly, B.T., Kieft, J.S., and Ramakrishnan, V. (2016). Large-Scale Movements of IF3 and tRNA during Bacterial Translation Initiation. Cell *167*, 133-144 e113.

Kaushal, P.S., Sharma, M.R., Booth, T.M., Haque, E.M., Tung, C.S., Sanbonmatsu, K.Y., Spremulli, L.L., and Agrawal, R.K. (2014). Cryo-EM structure of the small subunit of the mammalian mitochondrial ribosome. Proc Natl Acad Sci U S A *111*, 7284-7289.

Kim, D.E., Chivian, D., and Baker, D. (2004). Protein structure prediction and analysis using the Robetta server. Nucleic Acids Res *32*, W526-531.

Koc, E.C., and Spremulli, L.L. (2002). Identification of mammalian mitochondrial translational initiation factor 3 and examination of its role in initiation complex formation with natural mRNAs. J Biol Chem *277*, 35541-35549.

Lopez-Alonso, J.P., Fabbretti, A., Kaminishi, T., Iturrioz, I., Brandi, L., Gil-Carton, D., Gualerzi, C.O., Fucini, P., and Connell, S.R. (2017). Structure of a 30S pre-initiation complex stalled by GE81112 reveals structural parallels in bacterial and eukaryotic protein synthesis initiation pathways. Nucleic Acids Res *45*, 2179-2187.

Pettersen, E.F., Goddard, T.D., Huang, C.C., Couch, G.S., Greenblatt, D.M., Meng, E.C., and Ferrin, T.E. (2004). UCSF Chimera--a visualization system for exploratory research and analysis. J Comput Chem *25*, 1605-1612.

Punjani, A., Rubinstein, J.L., Fleet, D.J., and Brubaker, M.A. (2017). cryoSPARC: algorithms for rapid unsupervised cryo-EM structure determination. Nat Methods *14*, 290-296.

Rohou, A., and Grigorieff, N. (2015). CTFFIND4: Fast and accurate defocus estimation from electron micrographs. J Struct Biol *192*, 216-221.

Scheres, S.H. (2012). RELION: implementation of a Bayesian approach to cryo-EM structure determination. J Struct Biol *180*, 519-530.

Spremulli, L.L. (2007). Large-scale isolation of mitochondrial ribosomes from mammalian tissues. Methods Mol Biol *372*, 265-275.